Check for updates

ADVANCED PHYSICS RESEARCH Open Access
www.advphysicsres.com

Correlation of Structural Changes and Hydrogen Diffusion in Polycrystalline WO_3 Thin Films by Combining In Situ Transmission Measurements and Raman Spectroscopy

Markus S. Friedrich, Tim K. Hecker, Alexander G. Strack, Paul Tuchecker, and Peter J. Klar*

Diffusion in polycrystalline tungsten trioxide (WO_3) thin films is studied in a lateral geometry to better understand the impact of hydrogen-induced structural phase transitions on the diffusion. WO_3 thin films are coated with polymethylmethacrylate layer (PMMA). The latter is microstructured in such a way that a narrow stripe-like gap occurs in the PMMA layer exposing the surface of the WO_3 thin film. This stripe serves as the contact to the electrolyte in the intercalation experiment with hydrogen. After intercalation, the lateral diffusion of hydrogen inside WO_3 below the PMMA layer can be observed, increasing the analyzable path and time scale by several orders of magnitude compared to the film thickness, thus, significantly improving spatial and temporal resolution of in situ transmission and Raman measurements. Spatially resolved transmission measurements in the wavelength range of 633±55 nm show that the diffusion process is dependent on hydrogen concentration and exhibits two regimes describable by different diffusion coefficients. Time-resolved Raman spectroscopic measurements at different distances from the electrolyte contact area show that the switching between the two diffusion coefficients occurs at the phase transition from the orthorhombic to the tetragonal phase. The results are further supported by a simulation. The measurement approach is universally applicable for electrochromic films or multilayers.

1. Introduction

Changes in the crystal structure of tungsten trioxide (WO_3) due to the incorporation of hydrogen were first observed by Glemser and Naumann as early as 1951.[1] Hydrogen tungsten bronzes are formed by reduction of the tungsten ions,

$$\gamma H^+ + \gamma e^- + WO_3 \rightleftharpoons H_\gamma WO_3 \quad (1)$$

Hydrogen tungsten bronzes exhibit a wide range of crystal structures depending on hydrogen content and tungsten to oxygen stoichiometry.[2] For example, Cazzanelli et al. observe a monoclinic phase of the pristine polycrystalline samples which turns into orthorhombic and then tetragonal phase with increasing H-content γ. The orthorhombic to tetragonal transition takes place above $\gamma \approx 0.1$.[3,4] If the hydrogen concentration exceeds $\gamma = 0.5$, another phase transition into a cubic crystal structure will occur. At intermediate hydrogen concentrations, a tetragonal crystal structure is present. A distinction can be made between two different tetragonal phases. The transition between these two phases takes place at hydrogen concentrations of $\gamma \approx 0.25$.[3,5]

The diffusion of hydrogen in WO_3 thin films was first studied by Hitchman in 1977.[6] Since then, diffusion coefficients for hydrogen have been determined experimentally for many WO_3 thin films prepared in different ways.[7–12] Comparing the outcome of these studies yields a wide range of values of diffusion coefficients. This finding strongly suggests that microscopic and mesoscopic properties of the WO_3 thin film have a significant impact on hydrogen diffusion.

From a microscopic perspective, it is well established that hydrogen diffusion in WO_3 differs between amorphous and polycrystalline thin films.[13,14] It is also presumed, but not proven yet, that the crystal phase of polycrystalline WO_3 affects diffusion.[2,13]

Hydrogen diffusion in thin films is affected on the mesoscopic scale by properties of the deposited WO_3 film itself such as distributions of grain sizes and shapes, the type of grain boundary or porosity, but also by extrinsic properties such as the interface formed between WO_3 thin film and substrate or a top layer. These properties are mainly determined by the film deposition process. Microscopic and mesoscopic contributions to the diffusion behavior of hydrogen in WO_3 are hard to separate in experiments.

M. S. Friedrich, T. K. Hecker, A. G. Strack, P. Tuchecker, P. J. Klar
Institute of Experimental Physics I and Center for Materials Research (LaMa)
Heinrich-Buff-Ring 16, 35392 Giessen, Germany
E-mail: tim.hecker@exp1.physik.uni-giessen.de

The ORCID identification number(s) for the author(s) of this article can be found under https://doi.org/10.1002/apxr.202400019

© 2024 The Authors. Advanced Physics Research published by Wiley-VCH GmbH. This is an open access article under the terms of the Creative Commons Attribution License, which permits use, distribution and reproduction in any medium, provided the original work is properly cited.

DOI: 10.1002/apxr.202400019

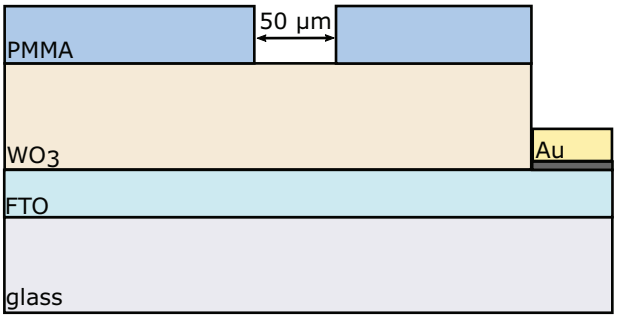

Figure 1. Schematic cross-section of a lithographically structured WO_3 thin-film sample.

This accounts to some extent for the large spread of data reported for the diffusion coefficients. In addition, when comparing the diffusion coefficients determined for polycrystalline films, the data are very likely also affected by the crystal phase transitions taking place because the channel widths between the network of WO_6 octahedra differ for the different crystal structures.[2]

Here, we present a method for studying hydrogen diffusion in polycrystalline WO_3 in the plane of thin films based on an approach previously introduced by some of us.[13] We expand the method by combining spatially and temporally resolved transmission (or absorption) measurements with spatially localized and temporally resolved Raman microscopic experiments in order to simultaneously assess hydrogen diffusion profiles and structural changes in the film plane. The lateral diffusion geometry is essentially realized by protecting the WO_3 surface only leaving a narrow stripe-like region where hydrogen may be incorporated into the WO_3 thin film. After the local incorporation of hydrogen into the WO_3, lateral diffusion in the film plane over distances of several 100 µm perpendicular to the stripe direction and over time scales of several 1000 s can be observed. In situ Raman measurements at different distances from the stripe-like gap allow us to identify the instants in time when the phase transition takes place at the different locations. This information can be correlated with the time evolution of the spatial diffusion profile obtained by analyzing the transmission data. The diffusion profiles show clear signatures of an alteration of the diffusion coefficient when a structural phase transition takes place with increasing hydrogen incorporation into the WO_3 thin film.

2. Results and Discussion

Figure 1 shows a schematic cross-section of a microstructured WO_3 thin film sample used in the experiments. These WO_3 thin-film samples are polycrystalline. Raman spectra clearly reveal that they exhibit grains in the monoclinic as well as in the orthorhombic phase in their pristine state (see Supporting Information). This confirms that the crystal structure of the film is not in the pure monoclinic phase as already reported previously for similarly prepared thin films.[15] The monoclinic grains transform into the orthorhombic phase when hydrogen incorporation starts. The sample preparation for the lateral diffusion experiment is somewhat similar to that of Vertes/Schiller.[8] However, in our case, the WO_3 thin film is covered with a polymethylmethacrylate (PMMA) layer. The PMMA layer is structured in such a way that the WO_3 film is exposed again in a stripe-like region with a width of 50 µm. In the electrochemical coloration and bleaching experiments, this stripe-like region serves as a contact to the electrolyte. During electrochemical cycling, hydrogen can be incorporated into the thin film or extracted out of the film only in this region because the remainder of the WO_3 film surface is protected by the PMMA layer. The hydrogen concentration gradient between the stripe-like region and the adjacent regions protected by the PMMA layer causes lateral diffusion of hydrogen perpendicular to the stripe-like gap, either side of the gap. We use an electrochemical cell with optical access, developed in house, for the transmission measurements. Thus, we can perform spatially resolved transmission experiments in situ during electrochemical cycling. Both, coloration and bleaching, can be observed which is of interest since they yield different pieces of information. The coloration process is limited by the hydrogen incorporation process hence determined by proton transport in the electrolyte contact area which follows the Butler–Volmer relation.[16] The bleaching process, however, is determined by a space-charge limited current due to different mobilities of electrons and protons (H^+).[10]

The changes in transmission of red light ($\lambda = (633 \pm 55)$ nm) during potentiostatic electrochemical coloration and bleaching, were monitored using the subtractive double spectrometer in imaging mode. A schematic drawing of the experimental setup can be seen in **Figure 2a**. The potential settings used for coloration and bleaching were −0.1 V vs. Ag/AgCl and 0.8 V vs. Ag/AgCl, respectively, as depicted in Figure 2b. The period of an electrochemical cycle is 4 h with 2 h for coloration and 2 h for bleaching.

Figure 2c–f shows the spatial dependence of the transmission through a micro-structured polycrystalline WO_3 thin film during the first two coloring and bleaching cycles. The transmission is characterized by the absorbance A of the film for electromagnetic radiation with a wavelength of (633 ± 55) nm, which is defined as

$$A\ (x) = -\ln\left(\frac{I\,(x)}{I_0}\right) \propto y\,(x) \tag{2}$$

where $I(x)$ is the transmitted intensity at position x of the sample and I_0 is the initially transmitted intensity at $t = 0$. Here, x denotes the distance in the direction perpendicular to the edge of the PMMA stripe from that edge to the spatial position of the measurement. Spatial profiles $A(x)$ derived at different times t correspond to hydrogen concentration profiles $y(x)$, if one assumes that Lambert–Beer's law holds.[13,15] This assumption is usually well justified within a single crystalline phase, if the spectral shape and the optical transitions involved in the absorption process are the same in the range of concentrations studied. The latter need not be the case in H_yWO_3 as phase transitions occur with y. A phase transition may change the electronic band structure which in turn may affect the optical transitions, that is, may introduce changes of the oscillator strengths, shifts or broadening of absorption bands. In the case of our H_yWO_3 thin film averaging over a wider spectral range compensates for such effects as is shown in (Figure S1, Supporting Information) for concentrations up to $y \cong 0.25$ with $y\,(x) = 0.4669\ A(x)$. These findings are also in good agreement with the results of Miyake.[17] The arrows in the four graphs indicate how $A(x)$ evolves during

© 2024 The Authors. Advanced Physics Research published by Wiley-VCH GmbH

27511200, 2024, 6, Downloaded from https://onlinelibrary.wiley.com/doi/10.1002/apxr.202400019 by Justus Liebig Universitaet Giessen, Wiley Online Library on [07/10/2024]. See the Terms and Conditions (https://onlinelibrary.wiley.com/terms-and-conditions) on Wiley Online Library for rules of use; OA articles are governed by the applicable Creative Commons License

27511200, 2024, 6, Downloaded from https://onlinelibrary.wiley.com/doi/10.1002/apxr.202400019 by Justus Liebig Universitaet Giessen, Wiley Online Library on [07/10/2024]. See the Terms and Conditions (https://onlinelibrary.wiley.com/terms-and-conditions) on Wiley Online Library for rules of use; OA articles are governed by the applicable Creative Commons License

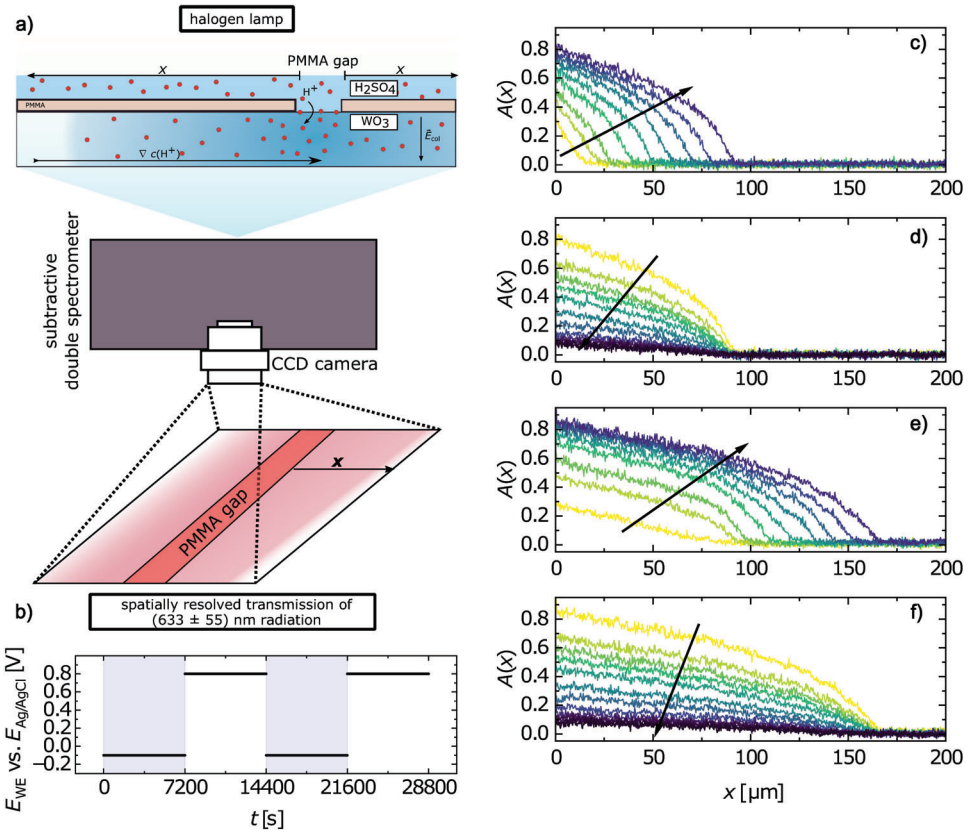

Figure 2. Schematic drawings of the setups for transmission spectroscopy in a) and the time-dependence of the voltage profile used for those measurements in b). Spatial absorbance profiles obtained by in situ transmission spectroscopy during electrochemical hydrogen insertion of a micro-structured WO_3 thin-film: c) first coloration step, d) first bleaching step, e) second coloration step, f) second bleaching step. The black arrows indicate the evolution over time.

coloration (graphs c) and e)) and during bleaching (graphs d) and f))

The absorption increases with time t for a given position x, as the hydrogen concentration y increases during coloration (graphs c) and e)). It can clearly be seen how the hydrogen diffuses laterally away from the PMMA gap as time progresses. The diffusion profile is somewhat unusual. The diffusion coefficients seem to differ at high and low absorbance. Furthermore, the behavior during the second coloration step differs from the first one in terms of the extension of the colored spatial region away from the gap below the PMMA layer. In the first coloration process in Figure 2c, the sample is colored to a distance of approx. 90 µm from the gap, in the second process, shown in Figure 2e, the sample is colored to a distance of almost 170 µm. A possible explanation is that the state of the sample after bleaching is not the same as in the pristine sample. This is suggested by two bleaching processes in Figure 2d,f which are similar and reveal that the sample is only almost completely bleached again after 2 h, in concordance with the Raman findings in (Figure S2, Supporting Information). We, therefore, believe that the thin film after bleaching is in an intermediate state closer to the orthorhombic phase than to the monoclinic phase of lower symmetry.

The difference in behavior between the bleaching and coloration processes is evident for both cycles. Unlike the diffusive behavior observed in coloration, the hydrogen appears to be extracted from the thin film during bleaching. This difference is due to the various limiting factors. The coloration is governed by the Butler–Volmer relation, while the bleaching is restricted by the space-charge limited current.

To further illustrate the change of diffusion behavior above a critical absorbance value of about 0.3, which correlates with a hydrogen concentration of $y \approx 0.14$ (see Equation (S1), Supporting Information), the results of the first coloration process are shown again in **Figure 3a**. At this hydrogen concentration, a transition between the orthorhombic to tetragonal crystal structure occurs.[1,3,5] The areas dominated by the different diffusion coefficients are linearly approximated in the graph. The region of lower absorbance is approximated by the dashed lines and the region of higher absorbance is approximated by the dotted-dashed lines.

The lines that belong together have a similar slope, further supporting the interpretation that this diffusion profile is one resulting essentially from two different diffusion coefficients assignable to the two crystalline phases. We estimated the initial diffusion coefficient D_i and subsequent diffusion coefficient D_s with an approach, that results in a formula similar to the mean square displacement for one dimension. The detailed derivation is given in the Supporting Information.

$$\Delta x^2 = 2D\Delta t \tag{3}$$

 © 2024 The Authors. Advanced Physics Research published by Wiley-VCH GmbH

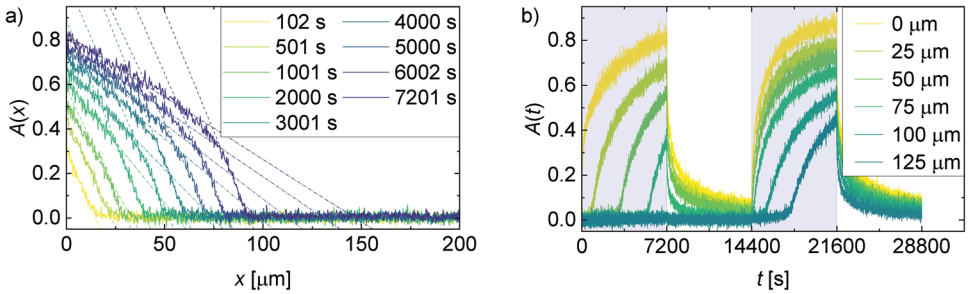

Figure 3. a) In situ transmission spectroscopic data for the first electrochemical coloration step with linear approximations of the different diffusion regimes. b) conversion of the spatial absorbance profiles to a time-dependent absorbance at different positions x during the first two coloring and bleaching cycles. The blue bars depict the coloration.

The range of the diffusion coefficients is given in **Table 1**. This findings are in good agreement with previous works on polycrystalline WO_3 thin films.[7,13,14]

In what follows, we will use Raman spectroscopy to confirm the assignment of the crystalline phase at a specific location x on the WO_3 thin film and to define the moment in time when a phase transition occurs locally, whilst recording simultaneously the transmitted intensity of the excitation laser through the WO_3 thin film and converting it into the time evolution of the absorbance $A(t)$ at this location. To prove the compatibility of the results obtained by transmission imaging spectroscopy with the Raman data, we convert the spatial absorbance profiles $A(x)$ obtained at different times t of the first two coloring and bleaching cycles into $A(t)$ curves for various x. The results are plotted in Figure 3b. It is easy to see that each time-dependent absorbance curve $A(t)$ starts to rise abruptly and very strongly at a specific point in time. This starting point in time is the later, the larger x, that is, the further away the location is from the stripe-like gap. After the initial rise, the $A(t)$ curve flattens out and starts to saturate. For example, during the first coloration step, no change at all can be observed at a distance of $x = 100$ µm and $x = 125$ µm, and the absorbance has not yet flattened out at a distance of $x = 75$ µm. It is also visible that during the bleaching step that follows the coloration is almost reversed. However, the absorbance is not quite zero for small x at the end of this bleaching step. This somewhat explains why the higher absorbance values can be obtained during the second coloration step and a change of absorbance is also observed at $x = 125$ µm in contrast to the first coloration step as discussed above.

We will turn now to the results of the in situ Raman and transmission spectroscopic results during electrochemical coloring and bleaching of micro-structured WO_3 films. In these experiments, the WO_3 thin films were colored by applying a coloring potential and a bleaching potential of −0.1 V vs. Ag/AgCl and 0.8 V vs. Ag/AgCl, respectively. The experimental setup is shown schematically in **Figure** 4a. To increase the stability of

Table 1. Estimation of initial and subsequent diffusion coefficients.

	D_i [cm^2 s^{-1}]	D_s [cm^2 s^{-1}]
1st cycle	$3.9 \times 10^{-10} - 7.4 \times 10^{-10}$	$6.0 \times 10^{-9} - 8.4 \times 10^{-9}$
2nd cycle	$2.0 \times 10^{-10} - 8.9 \times 10^{-10}$	$9.1 \times 10^{-9} - 1.6 \times 10^{-8}$

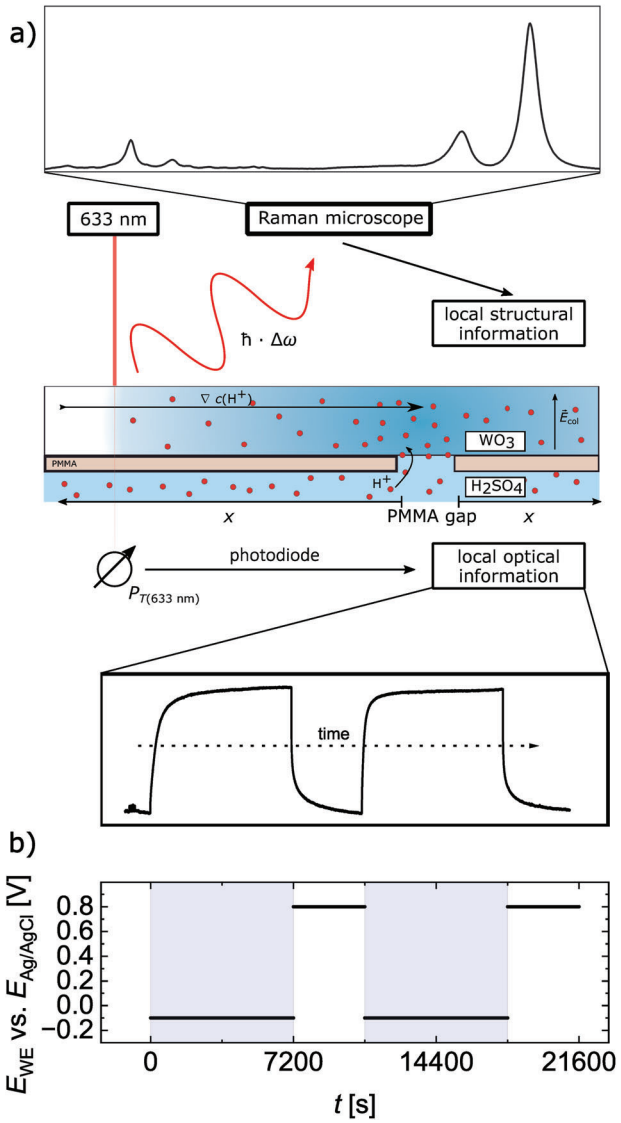

Figure 4. Schematic drawing of the setup for in situ Raman spectroscopy during electrochemical coloration and bleaching in a) and the time-dependent voltage profiles used for the performed measurements in b).

© 2024 The Authors. Advanced Physics Research published by Wiley-VCH GmbH

27511200, 2024, 6, Downloaded from https://onlinelibrary.wiley.com/doi/10.1002/apxr.202400019 by Justus Liebig Universitaet Giessen, Wiley Online Library on [07/10/2024]. See the Terms and Conditions (https://onlinelibrary.wiley.com/terms-and-conditions) on Wiley Online Library for rules of use; OA articles are governed by the applicable Creative Commons License

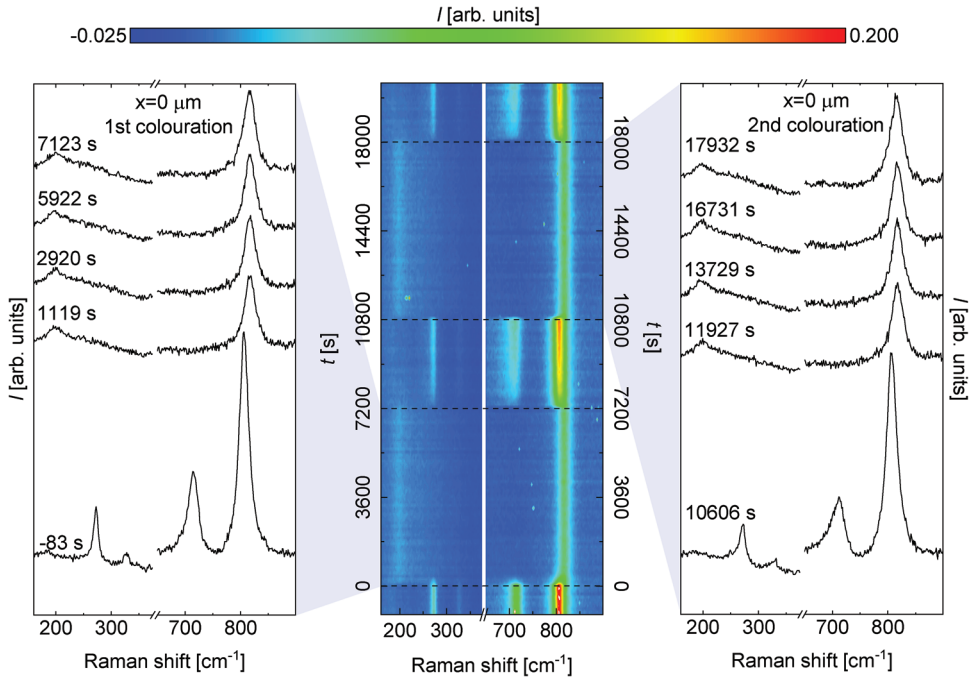

Figure 5. Raman contour-plots of the WO_3 thin-film at $x = 0$ µm distance from the PMMA gap (center). Individual Raman-spectra recorded during the first (left) and second (right) coloration step at $x = 0$ µm.

the electrochemical cell, the duration of the bleaching periods was reduced to 3600 s, while the duration of the coloration step was kept at 7200 s per cycle. The time-dependent voltage profile can be seen in Figure 4b. The measurements were carried out at different distances from the edge of the gap in the PMMA layer. It is worth noting that all the Raman and transmission data shown in this section were measured on different samples, underlining the high reproducibility of our extensive preparation and measurement approach.

At this point, the characteristics of the measurement method used should be explained once again. The covering of the WO_3 thin film with the microstructured PMMA layer defines the stripe-like region on the WO_3 surface where hydrogen incorporation is possible. Hydrogen entering the WO_3 film at this gap region will diffuse laterally inside the WO_3 thin film below the PMMA protective layer. This scenario basically provides a semi-infinite space of WO_3 either side of the gap and enables a more precise observation of the diffusion process. The distance along which free diffusion may take place is basically infinite compared to the film thickness, that is, the lateral extension of the sample is on the centimeter length scale whereas the thickness is a few hundred nanometers only. Given time, the hydrogen diffusion profile becomes very extended and the concentration gradients are rather small allowing us to study local changes at specific fixed positions on the sample as a function of hydrogen concentration. For example, this allows us to locally probe the change of the crystal structure by Raman microscopy while the hydrogen concentration changes during the coloration and bleaching cycle. This measurement at a fixed position ensures that the mesoscopic properties such as the grain structure remain the same over the entire measurement period and that the changes in the crystal structure can be directly correlated with the diffusion profile extracted via the change of the transmitted excitation laser intensity. **Figure 5** shows the Raman contour plot of the WO_3 thin film during two consecutive coloration and bleaching cycles, recorded at the center of the stripe-like gap in the PMMA film. Individual Raman spectra recorded during the first coloration step is shown on the left and those recorded during the second one on the right.

In both cases, the lowest spectrum (with time stamp −83 and 10606 s during the first and second cycle, respectively) is recorded prior to the application of the coloring potential. These spectra show the typical Raman signals of monoclinic/orthorhombic WO_3.[18] In particular, the modes at 272, 715, and 806 cm^{-1} are clearly visible, even the mode at 327 cm^{-1} can be recognized. Additional proof of the phase assignment is given by the Raman spectra in Figure S3 (Supporting Information).[4] It should be noted, that the area between wavenumbers 375 and 650 cm^{-1} is not shown in the contour plot and the individual Raman spectra, since there is no Raman signal visible in this range for the samples studied. The spectra recorded prior to the coloration period is very similar. Also in the temporal course of the coloring, the measured Raman signals behave similarly in both coloration processes. The modes at 272, 327, and 715 cm^{-1} disappear almost immediately, that is, within the first 1500 s after applying the coloration voltage. Furthermore, the mode that was originally found at 806 cm^{-1} is shifted to higher wavenumbers, more precisely 817 cm^{-1}, and significantly reduced in intensity. In addition, a broad mode appears at 198 cm^{-1} which was not present prior to coloration. These alterations yield Raman spectra characteristic for the tetragonal crystal structure of WO_3.[3] After this phase transition from orthorhombic to tetragonal, the Raman spectra remain the same until the end of the coloration step in both cycles. After the first bleaching step, the initial state seems

© 2024 The Authors. Advanced Physics Research published by Wiley-VCH GmbH

27511200, 2024, 6, Downloaded from https://onlinelibrary.wiley.com/doi/10.1002/apxr.202400019 by Justus Liebig Universitaet Giessen, Wiley Online Library on [07/10/2024]. See the Terms and Conditions (https://onlinelibrary.wiley.com/terms-and-conditions) on Wiley Online Library for rules of use; OA articles are governed by the applicable Creative Commons License

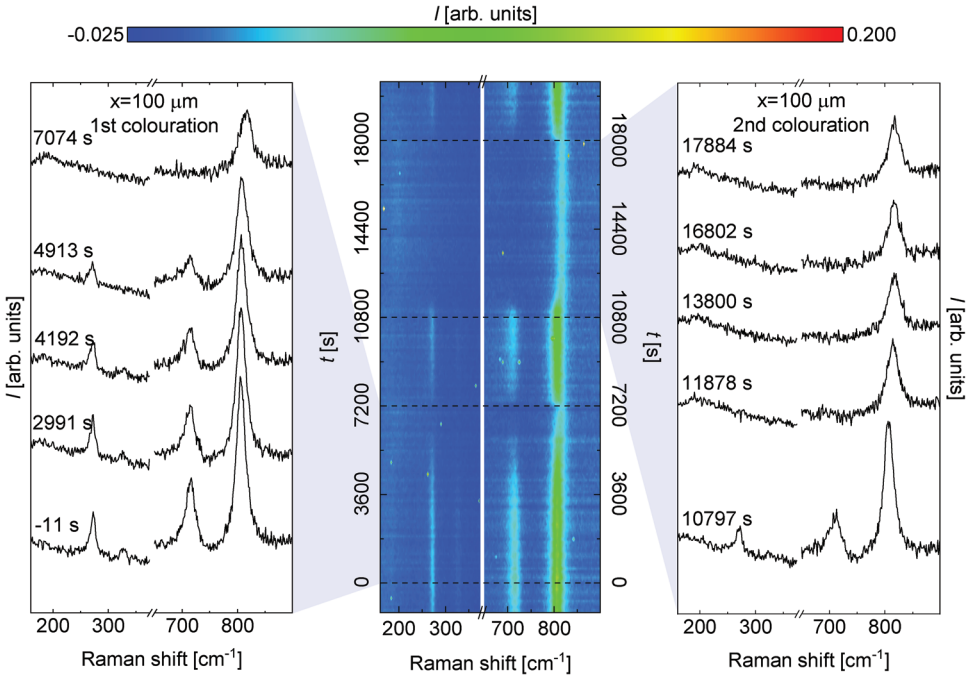

Figure 6. Raman contour-plots of the micro-structured WO_3 thin-film at $x = 100$ µm from the edge of the PMMA gap (center). Individual Raman-spectra recorded during the first (left) and second (right) coloration step at $x = 100$ µm.

to be nearly restored. However, the mode initially at 715 cm^{-1} has shifted to somewhat lower wavenumber 712 cm^{-1}, which may be a sign of stress or strain in the material[19] or a small part of the thin-film remaining in the tetragonal phase. This effect may also be related to residual hydrogen in the thin film after bleaching as already discussed above. Either way, the WO_3 thin film is back in its monoclinic/orthorhombic phase after the bleaching period in both cycles, but with a higher proportion of the orthorhombic phase (see Figure S3, Supporting Information).

We will now look at the situation at a location $x = 100$ µm away from the edge of the gap in the PMMA layer. At that position, the response to the hydrogen incorporation at $x = 0$ µm is delayed since hydrogen has to diffuse in the film plane to this location before coloration and phase transformation may take place. The impact on the crystal structure can be seen in the corresponding Raman contour plot of the WO_3 thin film shown in **Figure 6**. It is similar to Figure 5, but recorded at $x = 100$ µm. Again, individual Raman spectra recorded during the first and second coloration period are shown on the left and right, respectively.

The initial Raman spectrum taken before coloring (with time stamp −11 s) is similar to the corresponding one recorded directly in the PMMA gap and corresponds to the pristine sample. On coloration, the modes at 272, 327, and 715 cm^{-1} do not disappear immediately. Furthermore, the mode at 806 cm^{-1} does not immediately lose intensity or shift toward higher wavenumbers. Instead, the intensities of all modes in each spectrum shown decrease slowly as time progresses. Shortly before the end of the first coloration step (time stamp 7074 s), the modes 272, 327, and 715 cm^{-1} have vanished. Of the four original modes of the pristine sample, only the mode that initially was at 806 cm^{-1} can be seen but shifted to 817 cm^{-1}. In addition, a broad mode at 198 cm^{-1} starts to appear. Thus, in the first coloration step, it takes almost the full 7200 s for the hydrogen to diffuse laterally from the gap through the WO_3 thin film to the measurement position. This time span is needed to increase the hydrogen concentration at the measurement location to the level required for triggering the structural phase transition of the crystal structure from the monoclinic/orthorhombic phase to the tetragonal phase. The time span is much longer than at location $x = 0$ µm where the phase transformation takes place almost immediately after switching on the coloration voltage. This means the front, where the crystal structure changes, propagates along with the hydrogen as it laterally diffuses into the thin-film. This finding reflects that structural phase transition and hydrogen content are inherently related in hydrogen tungsten bronzes.

After the first bleaching step (spectrum recorded with time stamp 10797 s) the monoclinic/orthorhombic phase is present again, however, with a higher proportion of the orthorhombic phase (see Figure S3, Supporting Information). The mode at 327 cm^{-1} can only be just discerned and the modes at 272, 715, and 806 cm^{-1} are weaker in intensity than in the initial spectrum (time stamp −11 s, prior to the first coloration). This is a sign that the duration of the bleaching step of 3600 s is not sufficient to fully reverse the state of the thin film, as already indicated by the time-dependent absorbance measurements in Figure 3b. Thus, there remains residual hydrogen in the lattice after the first bleaching period. As a consequence, the thin film's behavior during the second coloration step is fundamentally different from that during the first one. It is somewhat similar to that observed at $x = 0$ µm in the gap area where the electrolyte is in direct contact with the film surface. The strong modes at 272 and 715 cm^{-1} which are indicative for the monoclinic/orthorhombic crystal structure vanish already after ≈1000 s during the second coloration period, in contrast to ≈5000 s during the first

© 2024 The Authors. Advanced Physics Research published by Wiley-VCH GmbH

27511200, 2024, 6, Downloaded from https://onlinelibrary.wiley.com/doi/10.1002/apxr.202400019 by Justus Liebig Universitaet Giessen, Wiley Online Library on [07/10/2024]. See the Terms and Conditions (https://onlinelibrary.wiley.com/terms-and-conditions) on Wiley Online Library for rules of use; OA articles are governed by the applicable Creative Commons License

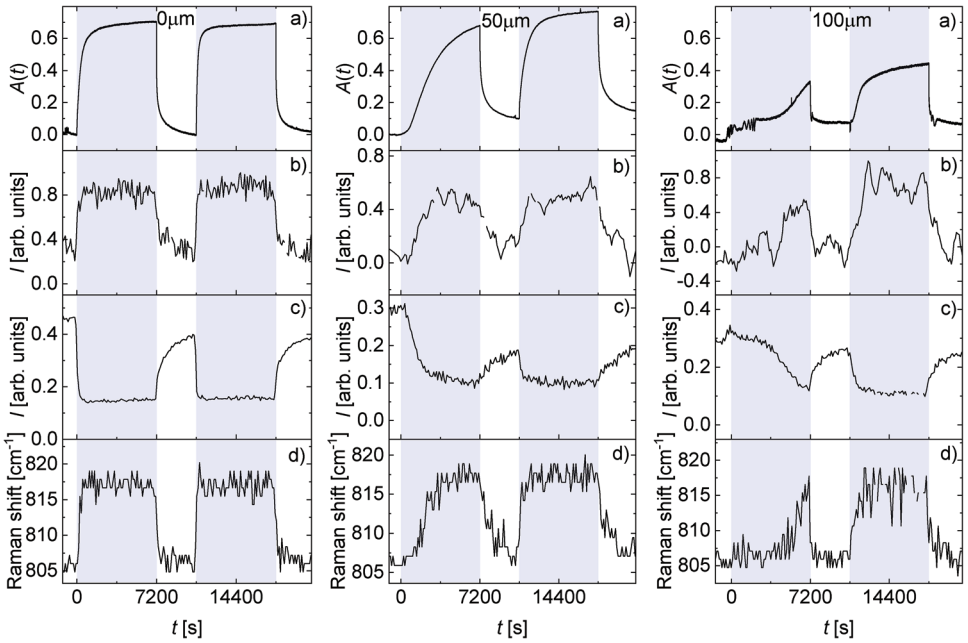

Figure 7. a) absorbance, b) Raman intensity of the mode at 198 cm^{-1}, c) peak Raman intensity of the mode initially at 806 cm^{-1}, and d) position of the peak of the Raman mode initially at 806 cm^{-1} for distances of 0, 50 and 100 µm from the PMMA gap. The blue bars correspond to the coloration steps.

coloration period. Within these 1000 s, the mode initially at 806 cm^{-1} decreases in intensity and shifts to a wavenumber value of 817 cm^{-1}. Thus, the changes of the crystal structure take place on a much shorter timescale than during the first coloration step due to the residual hydrogen concentration in the WO_3 layer or, possibly, a larger fraction of the orthorhombic phase is present prior to the second coloration step than in the pristine layer. After the tetragonal phase is established, no further alterations of the Raman spectrum are observed showing that the hydrogen concentration in the layer does not exceed $y = 0.5$.[1,3]

We will now address the temporal evolution of the Raman signals during the coloration/bleaching cycles. Changes of the Raman signals in terms of position and intensity may depend on intrinsic as well as external conditions. In particular, changes in intensity are often related to parameters such as alterations of the optical properties of the sample. For example, an increase of absorbance of the sample during the electrochemical coloration will also affect its reflectance and the volume probed in the Raman experiment.[20] The former alters the fraction of the laser intensity entering the sample and the latter decreases the number of potential Raman scattering centers and their Raman scattering cross-section. This means both will affect the signal intensity in the measured spectrum. The challenge is to identify changes in the Raman characteristics of the sample which are robust against absorbance changes. In our case, such characteristics are the shift of the Raman mode initially at 806 cm^{-1} and the appearance of the mode at 198 cm^{-1}, because both are clear signatures of the structural phase transition. Therefore, in **Figure 7** transmission data (in form of absorbance), the intensity of the Raman mode at 198 cm^{-1}, the intensity of the maximum of the Raman mode initially at 806 cm^{-1}, and the position in relative wavenumber of the maximum of the Raman mode initially at 806 cm^{-1} are displayed.

The absorbance profiles in Figure 7a are recorded at distances of $x = 0$, 50, and 100 µm from the edge of the stripe-like gap in the PMMA layer and are based on the measurement of the intensity of the transmitted excitation laser light in the Raman experiment. If compared with the transmittance curves in Figure 3b recorded with the imaging setup for spatially resolved transmission spectroscopy, one notes that the temporal dependence of the absorbance is very similar in both experiments, but the absolute values somewhat differ. The reason for the latter finding is that we use a spectrally broad probe light with wavelengths between 578 and 688 nm in the imaging transmission setup whereas the light source is monochromatic, that is 633 nm, in case of Raman setup. The average value taken in the measurement with probe light in the range from 578 to 688 nm differs from that obtained with monochromatic probe light of 633 nm because of the spectral dispersion of the absorbance.

However, the profile $A(x)$ of the absorbance curves, as discussed above, implies that their temporal behavior does not arise from a classical diffusion process with a constant diffusion coefficient. Instead, we assume that it arises from a process where the diffusion coefficient as a function of hydrogen concentration basically switches between two diffusion coefficients when the material undergoes a structural phase transition. The two virtually linear regions of the $A(t)$ curves can be correlated with the two linear regions of the $A(x)$ curves and thus with the two different diffusion coefficients. The reported insulator-metal transition cannot be considered a contributing factor to the change in diffusion coefficient.[21,22] This is because the electron mobility in pristine WO_3 is orders of magnitude higher than that of hydrogen ions.[23] This is further corroborated by the Raman experiments. In Figure 5, the structural phase transition in the gap region where the electrolyte is in direct contact with the WO_3 surface ($x = 0$ µm) takes place almost instantaneously at the

© 2024 The Authors. Advanced Physics Research published by Wiley-VCH GmbH

27511200, 2024, 6, Downloaded from https://onlinelibrary.wiley.com/doi/10.1002/apxr.202400019 by Justus Liebig Universitaet Giessen, Wiley Online Library on [07/10/2024]. See the Terms and Conditions (https://onlinelibrary.wiley.com/terms-and-conditions) on Wiley Online Library for rules of use; OA articles are governed by the applicable Creative Commons License

beginning of the coloration/bleaching cycle. In the further course of the coloration step, no more changes can be observed in the Raman spectrum, until the bleaching potential is applied. The structural phase transition at the beginning of coloration step is accompanied by a sharp increase of the absorbance. Afterward, the absorbance still increases, but with a much smaller slope. The behavior during the second coloration/bleaching cycle at $x = 0$ µm differs only marginally from that during the first cycle. However, it can be seen that the changes in absorbance are somewhat faster than in the first cycle. The measured Raman data correlates very well with the absorbance. In the areas where the absorbance of the WO_3 thin film exhibits a steep slope, the crystal structure also changes from monoclinic/orthorhombic to tetragonal, confirmed by the sudden shift of the mode originally at 806 to 817 cm^{-1} and the increase of intensity of the new mode at 198 cm^{-1}.

At a distance of $x = 50$ µm from the gap in the PMMA layer, the absorbance changes with time at a significantly slower rate than at $x = 0$ µm. During the first coloration/bleaching cycle, the change in the absorbance only just levels off toward the end of the coloration step. In conjunction with this, it can be seen from the Raman data that the crystal structure undergoes a rather continuous change and only reaches the state, that occurs almost instantaneously in the area where electrolyte and WO_3 are in direct contact, much later, that is, after approximately half of the coloration period. It should be emphasized that the shift of the mode, which originally was at 806 cm^{-1}, and also the emergence of the mode at 198 cm^{-1} does not happen abruptly, but rather continuously. So, there is no abrupt phase transition at a certain point in time, but the change of the crystal structure goes along with the continuous increase of the absorbance. This originates from the thin-films morphology with a distribution of grain sizes (see Figure S4, Supporting Information). In the second coloring/bleaching cycle, the changes at $x = 50$ µm occur more rapidly than in the first and the absorbance increases significantly faster at the beginning of the second coloration period. After the phase transition of the crystal structure has taken place, the absorbance still increases, but with a much smaller slope.

The continuous change of the crystal structure can be observed even more clearly at a distance of $x = 100$ µm from the gap in the PMMA layer. However, the state of the sample where the absorbance curve flattens out is not yet reached at $x = 100$ µm during the first coloration period. The Raman data confirm that the change in the crystal structure is not completed during the first coloration step. The intensity of the mode at 198 cm^{-1} has not reached saturation during this coloration step. Furthermore, the maximum of the mode, which is originally at 806 cm^{-1}, does not reach the wavenumber 817 cm^{-1} until the end of the first step. During the second coloration/bleaching cycle, the absorbance changes, and correspondingly the structural changes occur much faster and the phase transition into the tetragonal phase can be completed within the second coloration step.

For all three distances from the PMMA gap, it is confirmed that from the time when the phase transition to a tetragonal crystal structure is completed, the absorption curve flattens thus the environment with the higher diffusion coefficient is reached. It can thus be clearly seen that the change in the diffusion coefficient in WO_3 thin films is caused by a change in the crystal structure. One possible explanation is the higher symmetry of the tetragonal crystal structure compared to the monoclinic/orthorhombic one. In the latter, the WO_3 octahedra are less tilted or twisted against each other, which can lead to a reduction in the energy barrier for hydrogen transport. The fact that the structural changes are not fully reversed within the bleaching period increases the rate of change in subsequent coloring cycles. This irreversibility may be explained by the insulator-metal transition of WO_3 upon hydrogen insertion.[24] The phase transition of the crystal structure goes hand in hand with the continuous increase of hydrogen concentration and takes place at a critical hydrogen concentration. However, the critical hydrogen concentration may depend on the local environment such as strain state or grain size.

To further support our conclusions, a simulation of the diffusion process with a concentration-dependent diffusion coefficient was carried out using a Python program. The results of this simulation are shown in **Figure 8**.

Figure 8a,d shows the spatially resolved concentration $\gamma(x)$ for different moments in time t modeling the first and second coloration step. The steep diffusion front, which characterizes the area of the lower diffusion coefficient, and the quasi-linear part in the area of the higher diffusion coefficient can be clearly seen. This agrees well with the measurement data shown in Figures 2c–f and 3a. The values are in the same range as those determined by Burkhardt et al.[13] on similar samples. The graphs shown in Figure 8b,e represent the simulated time-dependent hydrogen concentrations $\gamma(t)$ at different distances x from the edge of the PMMA gap during the two bleaching steps. They are in good agreement with the measurement data recorded in Figures 3b and 7a, which show the corresponding absorbance profiles of the WO_3 thin film (which are proportional to the hydrogen content γ as described by Equation (2)) during bleaching. It is easy to see that a rapid increase in concentration can initially be observed near the gap. As the distance from the gap increases, the increase occurs later in time and the steepness of the increase decreases. In the range of the higher diffusion coefficient, the curves flatten out sharply and increase only slowly. The maximum concentration reached decreases with greater distances from the PMMA gap. Figure 8c,f shows the concentration-dependent diffusion coefficient used. In the first cycle, the region between 0 and 0.35 with a low gradient represents the transition from the monoclinic/orthorhombic phase to the orthorhombic one. After that, with increasing concentration the diffusion gradient rises with a steep gradient, representing the transition to the tetragonal phase. For the second cycle, the simulation was performed with the diffusion coefficient starting at a higher level for low concentrations, displaying the difference in crystal structure at the start of the second coloration cycle compared with the pristine sample.

3. Conclusion

With the measurement method presented, changes in diffusion can be traced back to changes in the crystal structure. As the diffusion profile and crystal structure changes are correlated at the same locations on the thin film. Thus, using this approach, the diffusion coefficients of the different crystalline phases of WO_3 can be compared within one and the same sample, that is, for the same mesoscopic structure. Based on the data collected in this way, it can be well concluded that the diffusion profile of hydrogen in a WO_3 thin film with essentially two different

© 2024 The Authors. Advanced Physics Research published by Wiley-VCH GmbH

27511200, 2024, 6, Downloaded from https://onlinelibrary.wiley.com/doi/10.1002/apxr.202400019 by Justus Liebig Universitaet Giessen, Wiley Online Library on [07/10/2024]. See the Terms and Conditions (https://onlinelibrary.wiley.com/terms-and-conditions) on Wiley Online Library for rules of use; OA articles are governed by the applicable Creative Commons License

27511200, 2024, 6, Downloaded from https://onlinelibrary.wiley.com/doi/10.1002/apxr.202400019 by Justus Liebig Universitaet Giessen, Wiley Online Library on [07/10/2024]. See the Terms and Conditions (https://onlinelibrary.wiley.com/terms-and-conditions) on Wiley Online Library for rules of use; OA articles are governed by the applicable Creative Commons License

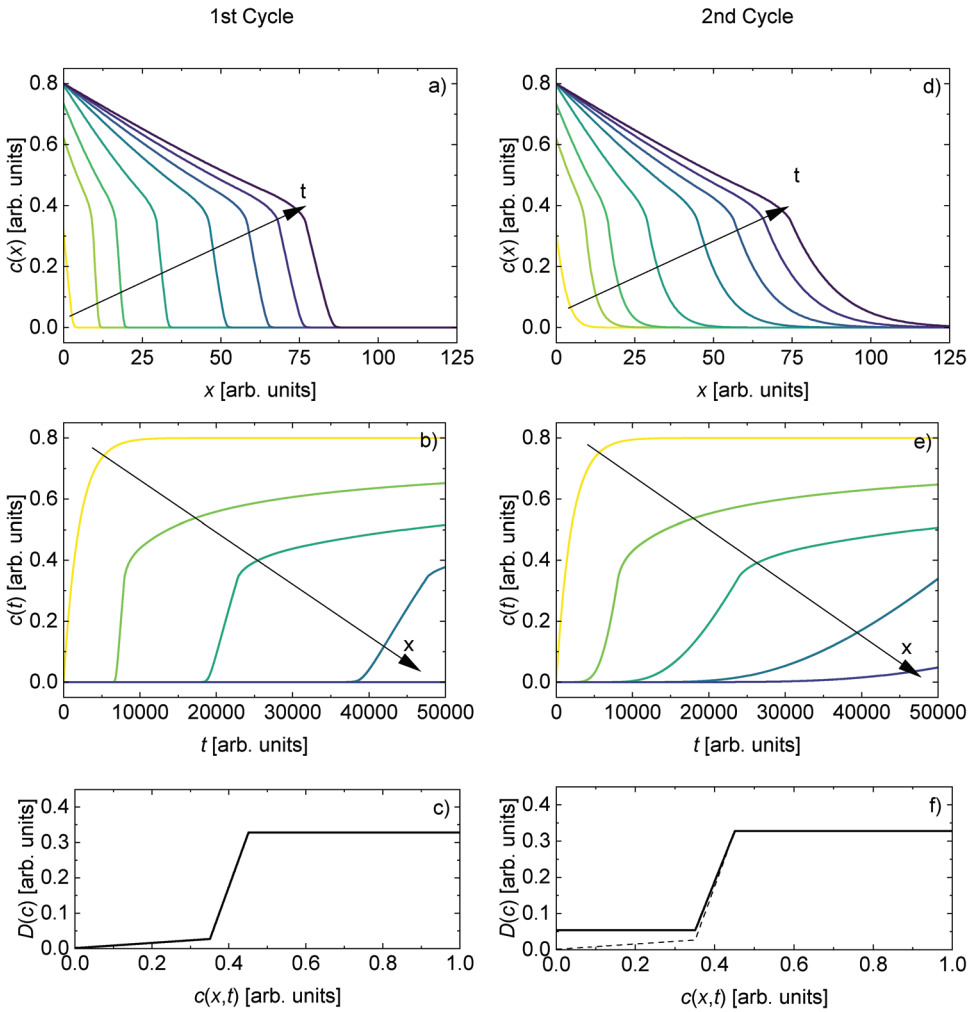

Figure 8. Simulation of a diffusion process with a concentration-dependent diffusion coefficient for the first and second coloration cycles: a,d) spatial concentration profiles at different times *t*, b,e) temporal evolution of the concentration at different distances *x*, c,f) concentration dependent diffusion coefficient assumed in the simulation.

diffusion coefficients can be explained by a phase transition from a monoclinic/orthorhombic crystal structure to a tetragonal crystal structure of higher symmetry. This phase transition is caused by the incorporation of hydrogen into the crystal lattice. On the time scales of the measurements performed, this process is not completely reversible, that is, the fraction of the orthorhombic phase at low hydrogen concentrations increases after bleaching. It remains to be clarified whether another abrupt change of the diffusion coefficient will occur at higher coloring potentials when the phase transition from the tetragonal into the cubic phase of WO_3 is expected.

4. Experimental Section

Sample Preparation: Formerly commercially available amorphous WO_3 films deposited on fluorine-doped tin oxide (FTO) covered glass substrates (received from "*eControl*") were used as starting point of our samples. An FTO film serves as current collector/electrical contact of the electrochromic thin film. To uncover the FTO film underneath the WO_3 film for contacting, a stripe along the edge of the substrate, with a width of roughly 2 mm, was treated with potassium hydroxide (1.938 mol L^{-1}, ≥ 85 % purity, purchased from "*Roth GmbH + Co KG*") solution, to etch off the WO_3 in this area.

Afterward, the sample was heated in a "*Nabertherm*" furnace with air as atmosphere at a rate of 100 °C h^{-1} to a temperature of 450 °C. The temperature was held for 1 h to crystallize the WO_3 thin-film. Following this, the samples slowly cooled down to room temperature inside the furnace. The crystallized WO_3 thin-films possessed a thickness of 560 ± 32 nm.

To enhance the electrical contacting of the thin-film, 6 ± 3 nm Cr and 100 ± 15 nm Au were deposited by thermal evaporation on the blank FTO surface. For the deposition a thermal evaporation system "E12E4" from "*Edwards*" was used. To prevent the deposition of metal on top of the WO_3 surface, this area was covered by aluminum foil during the thermal evaporation process.

In a micro structuring process, a 200 nm thick PMMA film on top of the sample was structured in order, to create a well-defined line-shaped contact area for the electrolyte in the electrochemical coloration experiments. For this purpose, 150 µL of a solution of 4 % PMMA in anisole (purchased from "*MicroChem Corp.*") was deposited by spin coating on top of the sample. The rotation speed was set to 3000 rpm and the spin coating process lasted for 45 s. As spin coater a "Delta6 RC" by "*SÜSS MicroTec AG*" was used. Afterward, the whole sample was transferred to a hot plate whose

 © 2024 The Authors. Advanced Physics Research published by Wiley-VCH GmbH

temperature was set to 180 °C and was baked for 2 min in the air as atmosphere. The PMMA film was then structured by electron beam lithography using a "XeDraw 2" electron beam lithography system by "*XENOS*" which was integrated into a "JSM 7001F" scanning electron microscope by "*JEOL*". A line pattern with a width of 50 µm across the sample was exposed with an acceleration voltage of 15 kV and a beam current of 200 pA. Afterward, the PMMA in this area was removed by developing the resist in a mixture of isopropyl alcohol and deionized water with a volume ratio of 2:1 for 45 s.

Electrochemical Hydrogen Insertion: Two specially designed electrochemical cells were used for electrochemical investigation of the electrochromic behavior. They were built in a house with three-electrode arrangement. The cells enable in situ spectroscopy during electrochemical experiments. The cells were very similar to the cells used in the previous work.[13] In the setup the micro-structured samples served as working electrode, a platinum tube was used as counter electrode and a Ag/AgCl "Driref-450" microelectrode from "*World Precision Instruments Inc.*" was used as reference electrode. The potential of the reference electrode against the standard hydrogen electrode is $E_{\mathrm{Ag/AgCl\,vs.\,SHE}} = 0.197$ V. As electrolyte solution eluent H_2SO_4 (0.1 mol L^{-1}), purchased from "Sigma–Aldrich", was filled into the cell. A "SP-150" potentiostat from "*Biologic*" was used to apply the coloration and bleaching potential.

In Situ Transmission Spectroscopy: To investigate the coloration state, the samples were illuminated during coloration and bleaching with a halogen lamp and the spatial and temporal changes of the transmitted light, and therefore the hydrogenation of the structured samples in a spatially and timely resolved manner, were analyzed. For this purpose, the transmitted light was focused by a tenfold magnification objective onto a 6.0 mm entrance slit of a subtractive double spectrometer in Czerny-Turner-geometry of the type "Spex 1680 b" from "*Horiba Jobin Yvon GmbH*". The intermediate slit with a width of 2.2 µm served as a bandpass filter, that could only be passed by light with a wavelength of $\lambda_{\mathrm{trans}} = (633 \pm 55)$ nm. The intensity distribution of the transmitted light was detected by a "ICX258AL" sensor by "*Sony*" in combination with a "pco. 1400" CCD camera purchased from "*PCO AG*". The image size was (1392 x 1040) pixels, with a pixel size of (6.45 x 6.45) μm^2. The images were recorded over an integration time of 500 ms followed by a resting time of 2 s. To analyze pixel lines perpendicular to the PMMA gap a virtual instrument created with the software "LabVIEW" from "*National Instruments Corp.*" was used. This experiment was performed during coloration and bleaching of the films with an applied coloration potential of −0.1 V vs. Ag/AgCl and a bleaching potential of 0.8 V vs. Ag/AgCl, to insert and remove hydrogen into and from the micro-structured WO_3 thin film, respectively. Both potentials were applied for 2 h each. The experiment was performed over three coloring and bleaching cycles.

In Situ Raman Spectroscopy: For Raman experiments, a Raman spectrometer "In-Via", equipped with a charge-coupled device (CCD) camera, by "*Renishaw*" was used. The excitation wavelength of the laser light was chosen to be $\lambda_{\mathrm{Laser}} = 633$ nm. The Raman experiments were performed in backscattering geometry and data was recorded in confocal mode. During these experiments a "PM100D" power meter equipped with a "S130VC-SP2" power sensor, both manufactured by "*Thorlabs GmbH*" was used, to record changes in the transmission of the laser light through the sample

SEM Measurements: Scanning electron microscopy (SEM) imaging was carried out using a "Zeiss Merlin HRSEM".

Supporting Information

Supporting Information is available from the Wiley Online Library or from the author.

Acknowledgments

The authors are grateful for financial support in terms of the European Regional Development Fund granted by the State of Hessen.

Conflict of Interest

The authors declare no conflict of interest.

Data Availability Statement

The data that support the findings of this study are available from the corresponding author upon reasonable request.

Keywords

concentration dependent diffusion, in situ transmission spectroscopy, in situ Raman spectroscopy, electrochromism, tungsten trioxide

Received: February 12, 2024
Revised: March 8, 2024
Published online: April 11, 2024

[1] O. Glemser, C. Naumann, *Z. Anorg. Allg. Chem.* **1951**, *265*, 288.
[2] L. Bartha, A. B. Kiss, T. Szalay, *Int. J. Refract. Met. Hard Mater.* **1995**, *13*, 77.
[3] O. Pyper, A. Kaschner, C. Thomsen, *Sol. Energy Mater. Sol. Cells* **2002**, *71*, 511.
[4] E. Cazzanelli, C. Vinegoni, G. Mariotto, A. Kuzmin, J. Pujans, *Solid State Ionics* **1999**, *123*, 67.
[5] U. Opara Krasovec, A. Surca Vuk, B. Orel, *Electrochim. Acta* **2001**, *46*, 1921.
[6] M. Hitchman, *J. Electroanal. Chem.* **1977**, *85*, 135.
[7] M. Hitchman, *Thin Solid Films* **1979**, *61*, 341.
[8] A. Vértes, R. Schiller, *J. Appl. Phys.* **1983**, *54*, 199.
[9] S. K. Mohapatra, *J. Electrochem. Soc.* **1978**, *125*, 284.
[10] B. W. Faughnan, R. S. Crandall, M. A. Lampert, *Appl. Phys. Lett.* **1975**, *27*, 275.
[11] G. Nagy, R. Schiller, *Int. J. Hydrogen Energy* **1989**, *14*, 567.
[12] C. Bohnke, O. Bohnke, *J. Appl. Electrochem.* **1988**, *18*, 715.
[13] S. Burkhardt, M. T. Elm, B. Lani-Wayda, P. J. Klar, *Adv. Mater. Interfaces* **2018**, *5*, 1701587.
[14] J. Randin, R. Viennet, *J. Electrochem. Soc.* **1982**, *129*, 2349.
[15] S. Darmawi, S. Burkhardt, T. Leichtweiss, D. A. Weber, S. Wenzel, J. Janek, M. T. Elm, P. J. Klar, *Phys. Chem. Chem. Phys.* **2015**, *17*, 15903.
[16] R. S. Crandall, B. W. Faughnan, *Appl. Phys. Lett.* **1975**, *26*, 120.
[17] K. Miyake, H. Kaneko, M. Sano, N. Suedomi, *J. Appl. Phys.* **1984**, *55*, 2747.
[18] M. F. Daniel, B. Desbat, J. C. Lassegues, B. Gerand, M. Figlarz, *J. Solid State Chem.* **1987**, *67*, 235.
[19] C. Rice, R. J. Young, R. Zan, U. Bangert, D. Wolverson, T. Georgiou, R. Jalil, K. S. Novoselov, *Phys. Rev. B* **2013**, *87*, 081307.
[20] D. F. Shriver, J. B. R. Dunn, *Appl. Spectrosc.* **1974**, *28*, 319.
[21] X. Leng, J. Pereiro, J. Strle, G. Dubuis, A. T. Bollinger, A. Gozar, J. Wu, N. Litombe, C. Panagopoulos, D. Pavuna, I. Božovic´, *npj Quantum Mater.* **2017**, *2*, 35.
[22] K. Yoshimatsu, T. Soma, A. Ohtomo, *Appl. Phys. Express* **2016**, *9*, 075802.
[23] X. Meng, F. Quenneville, F. Venne, E. Di Mauro, D. Işık, M. Barbosa, Y. Drolet, M. N. Natile, D. Rochefort, F. Soavi, C. Santato, *J. Phys. Chem. C* **2015**, *119*, 21732.
[24] E. V. Miu, G. Mpourmpakis, J. R. McKone, *ACS Appl. Mater. Interfaces* **2020**, *12*, 44658.

© 2024 The Authors. Advanced Physics Research published by Wiley-VCH GmbH

27511200, 2024, 6, Downloaded from https://onlinelibrary.wiley.com/doi/10.1002/apxr.202400019 by Justus Liebig Universitaet Giessen, Wiley Online Library on [07/10/2024]. See the Terms and Conditions (https://onlinelibrary.wiley.com/terms-and-conditions) on Wiley Online Library for rules of use; OA articles are governed by the applicable Creative Commons License